Electron Beam Simulations REU Program at Columbia University - Nevis Labs

Isabel Hahn^{1,2}

¹Pomona College ²Nevis Labs

August 6, 2024

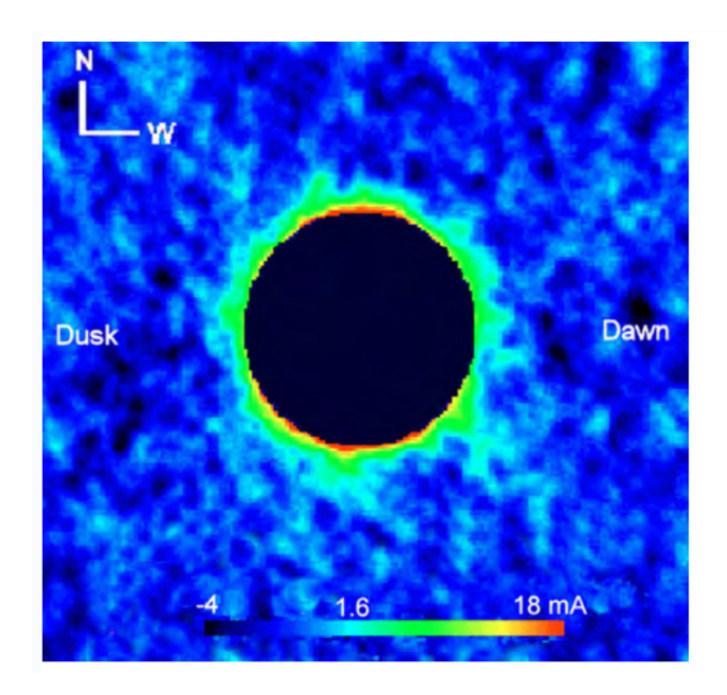
Abstract

Mercury has a sodium exosphere, which has been proven via ground based observations. The mechanism of elevation is believed to be solar wind ion sputtering. Currently, the Mercury Planetary Orbiter of the BepiColombo mission is en route to Mercury to study its exosphere, and in order to accurately interpret this data we need to understand the physical process that created it. Sputtering from ion irradiation is well studied with solid materials, but not with loose powders. We create a laboratory simulation of ion irradiation of loose powders to resemble Mercury's regolith. A complication of irradiating loose powders is sample charging, which may be mitigated by the use of an electron flood gun. I used SIMION, and ion trajectory simulation, to simulate the behavior of the electron flood gun directed onto a charged beam spot to determine the yield of electrons that reach the beam spot and would theoretically neutralize it. I found that the electrons are not always attracted to the positive beam spot, particularly at very high beam spot voltages. I also found that this effect is dependant on the beam geometry, and moving the flood gun to an alternate port location could reduce the intensity of repulsive electron behavior.

Contents

1	\mathbf{Intr}	roduction	3
	1.1	Planetary Science: Mercury's Sodium Exosphere	3
	1.2	The Phoenix Project	4
2	The	e Experiment	4
	2.1	The Apparatus	4
	2.2	The Target Chamber	4
	2.3	The Sample	7
		2.3.1 Sample Reduction	8
		2.3.2 Sample Charging	9
		2.3.3 Electron Flood Guns	9

3	SIMION 10				
		Background Information			
	3.2	Geometry	11		
	3.3	First Round of Data	11		
		3.3.1 Kinetic Energy Analysis	12		
		3.3.2 Positional Correlation	15		
		3.3.3 Electric Field Asymmetry	16		
	3.4	Alternate Beam Port	17		
	3.5	Beam Re-Shape	17		
4	Con	nclusion	21		
5	Ack	nowledgements	21		



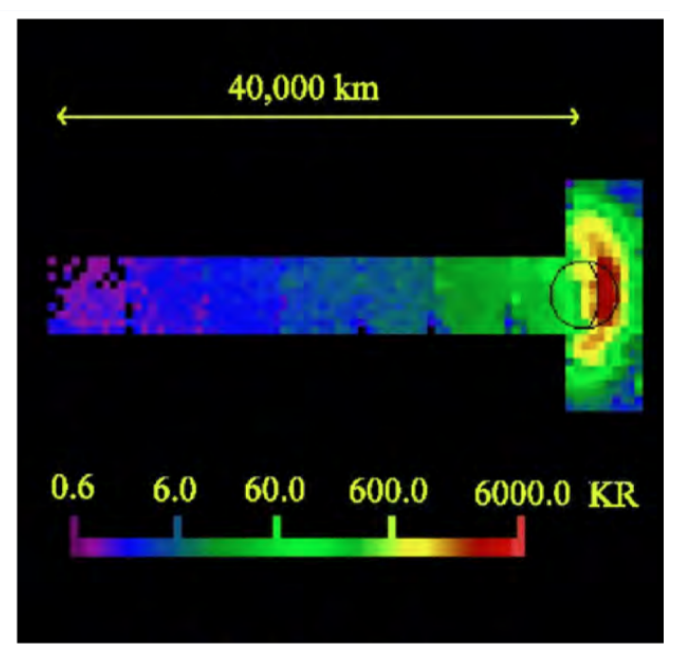


Figure 1: Left: Na abundance in Mercury's exosphere, captured during the solar transit on November 8th 2006 with the Dunn Solar Telescope (Ref. [8]). The color map shows the Na absorption equivalent width in mÅ. The blue background is the solar disk, and has a root-mean-square noise level of 1.6 mÅ. Right: Image of Na D₂ emission intensity observed on May 26th 2001 with the McMath-Pierce Solar Telescope (Ref. [7]). The emission intensity is measured in kilorayleighs (kR). The black circle outlines Mercury, and the crescent identifies the dawn terminator. The image extends 40,000 kilometers din the anti-sunward direction to capture the Na D₂ emissions from both the planet's exosphere and the anti-sunward tail.

1 Introduction

1.1 Planetary Science: Mercury's Sodium Exosphere

A big component of planetary science is studying planetary atmospheres. Atmospheres give us clues about surface mineralogy on a planet, because the majority of the material in the space surrounding a planet comes from the planet itself. This allows us to constrain planetary formation models, and better understand solar system formation and evolution.

Mercury has a tenuous and collisonless atmosphere called an exosphere (Ref. [2]). From ground based observations, we know it is primarily sodium and helium. In Figure 1, the right image is the observed spectra of Mercury transiting the sun, and depicts a high concentration of sodium in Mercury's exosphere particularly near the planet's North and South poles. The right image shows the Na D_2 line emission intensity in kilorayleighs on mercury and its anti-sunward facing tail. In order to eject from the planet's gravitational hold, these sodium particles were acted upon with very high energy.

This sodium exosphere is believed to be caused by solar wind ion sputtering, a process in which H^+ and He^{2+} ions from the solar wind collide with the planet's surface at very high energies and eject atoms. (Ref. [3], [4]) The amount of energy that is transferred to the ejected atoms is sufficient in some cases to free the atom from the planet's gravitational hold. Combined with pressure from the solar wind acting upon the ejected atoms, an anti-sunward tail of ejected sodium atoms is formed downwind of the planet. Solar wind travels parallel to a planet's magnetic field, making the

magnetospheric cusps an ideal point of entry since the magnetic fields here are perpendicular to the surface. This corresponds with the high concentration of sodium we observe at Mercury's North and South pole.

In addition to the ground based observations of Mercury's exosphere mentioned above, there are space missions imaging the planets exosphere as well. Particularly relevant at this time is the BepiColombo Mission, of which the Mercury Magnetospheric Orbiter (MMO) carrying the Mercury Sodium Atmosphere Spectral Imager (MSAI) is set to reach its final orbit around Mercury in 2025. Data from these missions will be used to study Mercury's sodium exosphere and the process of ion sputtering on the planets surface. (Ref. [10]) The data from this mission will be high quality, but we need to thoroughly understand the physical processes behind the data in order to develop a high quality analysis. There are many uncertainties in our understanding of the solar wind ion sputtering process that created Mercury's exosphere, particularly in relation to the behavior of loose powders. One way to better understand this process is to recreate it in a controlled laboratory setting, where we can directly observe it.

1.2 The Phoenix Project

Ion sputtering is well studied in a laboratory setting with solid materials, however there is little information about ion sputtering with loose powders. The PHOENIX project is intended to simulate the process of ion sputtering on loose powders, and determine parameters such as sputtering yield and angular distribution that will allow data from the Bepicolombo mission to be interpreted more accurately.

2 The Experiment

2.1 The Apparatus

The Phoenix apparatus (Ref. [1]) utilizes a 20 keV Kr⁺ beam that is guided through a series of optics, monitors, and beam steerers and into the target chamber where it will irradiate a target sample at a polar angle of 45°. The target rests inside the target chamber and is a sample intended to represent the surface of Mercury. It is very large and consists of many tediously aligned and calibrated components.

Figure 3 depicts a diagram of the apparatus, including labels of each component, as well as an image of the physical apparatus in the lab. For the scope of this report, we are mainly focusing on the target chamber of the apparatus.

2.2 The Target Chamber

The target chamber (Fig. 3) is where the ion irradiation will occur. It is completely sealed and equipped with a turbo vacuum pump to simulate the vacuum environment of space. The ion beam enters through one of the many side ports, and is aligned to hit the center of the sample within.

The sample, as depicted in Fig. 4 is held in a sample holder inside the target chamber. It consists of a sample stage that has dimensions of one inch by two inches by two mm, and a sample cup that has an interior diameter of 36 mm and a thickness of two mm. The sample cup is mounted onto the sample stage, which is then mounted in the target chamber. Mounted over the sample holder is the catcher dome, which is visible in Fig. 3. The dome has a main opening for the beam to pass through, and a series of circular holes to hold catcher foils, which are depicted in Fig. 5. The purpose of the

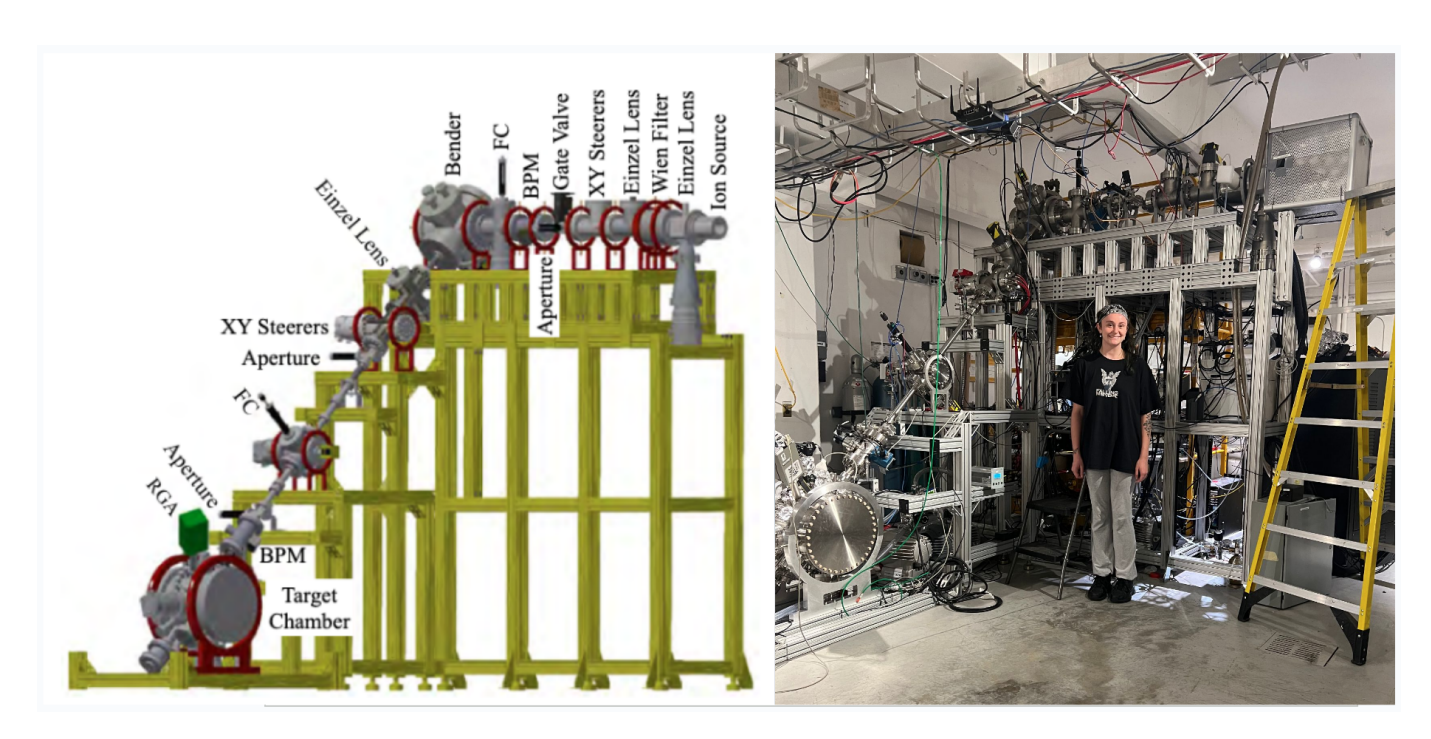


Figure 2: Right: A labeled diagram of the apparatus and its main components. Left: An image of the apparatus in the laboratory, with a person for scale who is approximately five feet and eight inches tall.

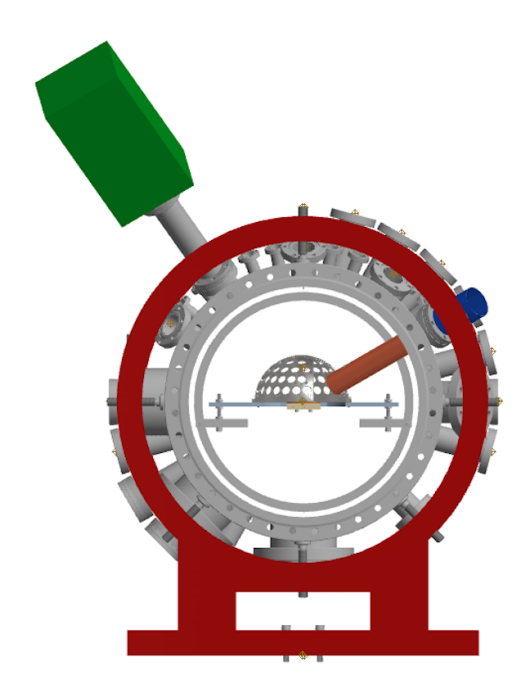


Figure 3: Diagram of the target chamber and interior components, side view.

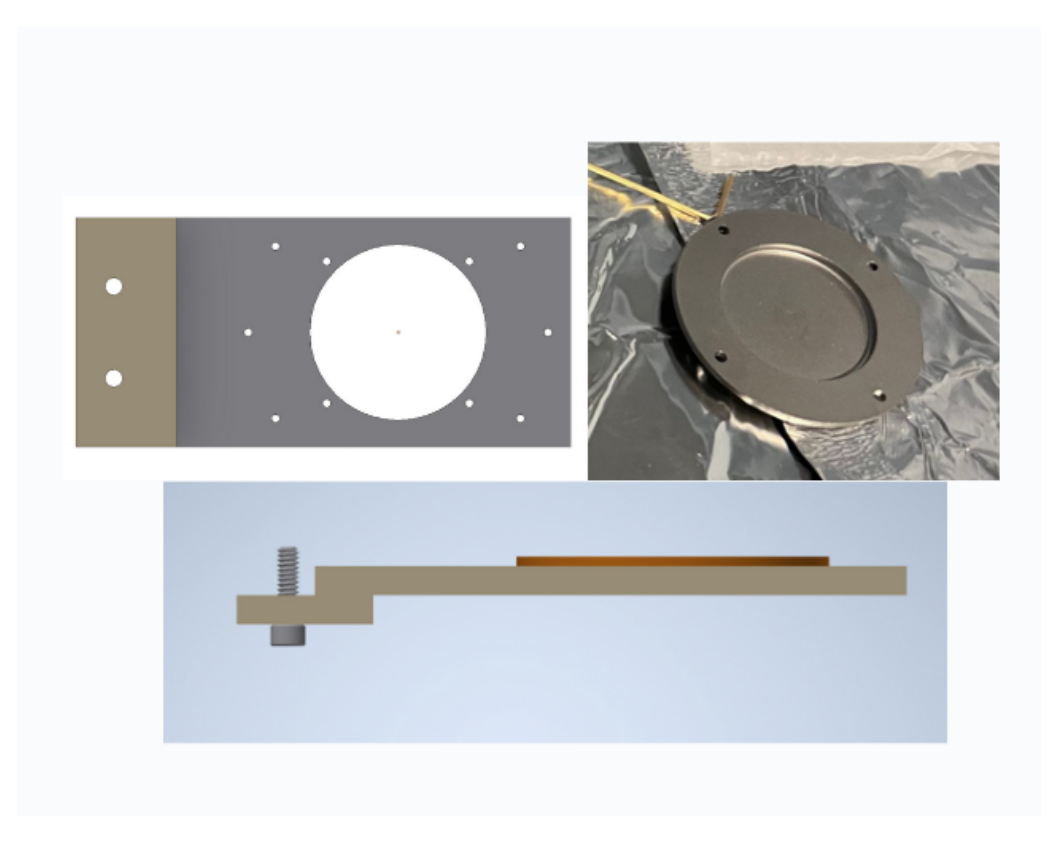


Figure 4: Top Left: Diagram of sample stage from above. Top Right: Image of sample cup in the laboratory. Bottom: Side view of fully assembled sample holder. The sample cup rests in the hole of the sample stage, and with its rim resting on the sample stage.

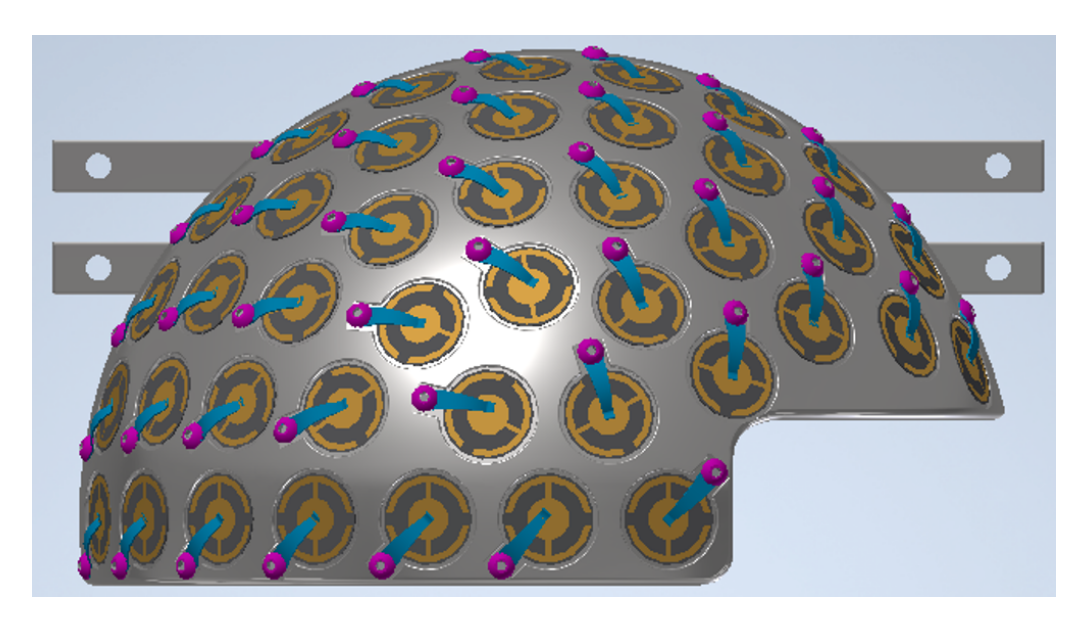


Figure 5: Diagram of half of the dome with all catcher foils installed, top view. In the experiment, the dome is a full half sphere, with an opening for the beams to enter.

catcher foils is to catch atoms that are sputtered from the sample, giving us information about not only the sputtering yield, but also the sputtering angular distribution as they are situated at a range of azimuthal and polar angles across the dome. All components in the target chamber are grounded, including the chamber itself.

2.3 The Sample

The apparatus has successfully irradiated a solid copper slap (Ref. [1]), which was chosen as a sample because the behavior of solid copper in irradiation experiments is well studied and understood. The next step is to use loose copper powder, as it can be compared to the results from the copper slab. The use of copper is not intended to directly represent the surface minerology of Mercury. It is a proof of concept to ensure that the apparatus functions properly and is capable of irradiating loose powders. Once the apparatus successfully irradiates the copper powder, we will move on to a more complex sample that is closer to the actual chemical composition of the hermian regolith, most likely a plagioclase feldspar. (Ref. [6])

The copper powder we are using for our sample has spherical grains. To prepare the sample for the experiment, we must do two things; separate ideal grain sizes, and remove the oxide layer.

The target range of grain sizes for this experiment is 53 microns to 90 microns. This target range was selected to most closely match the range of grain sizes in Mercury's regolith (Ref. [2]). There have been no sample return missions from Mercury, however we make an interpretation of the grain sizes in Mercury's regolith based off of samples from the Moon's regolith. Both surfaces experience similar solar wind ion bombardment, therefore both regoliths should have a similar range of grain size.

To obtain this grain size range, we purchase the closest available copper powder to this range. We then use a stack of special sieves that have mesh sizes of 90 and 53 microns. After the sieving process, the grains that remain in the area between the two sized sieves are of the correct grain size range (Fig. 6).



Figure 6: From left to right: Reduced and sieved Cu sample, Sieved CuO sample, sieve stack (90 micron screen on top, 53 micron screen in middle, catcher tray on the bottom), and the CuO sample as it was purchased.

2.3.1 Sample Reduction

Once we have obtained the correct grain sizes, we may move on to the next step which is to remove the oxide layer. We conduct a reduction experiment using the facilities at Lamont Laboratories.

The reaction is: $CuO_{(s)} + H_{2(g)} \xrightarrow{heat} Cu_{(s)} + H_2O_{(g)}$.

The procedure of the experiment is:

- 1. Clean up the fume hood and put the stand and clamp inside the fume hood.
- 2. Weigh the reduction tube empty.
- 3. Place about 3 g of Cu/CuO along the base of the Pyrex boiling tube (reduction tube) so that it is spread out over a length of about 4 cm centered on the middle of the tube. This is to ensure that it will not be necessary to heat too close to the rubber stoppers.
- 4. Reweigh and note the mass of the tube plus Cu/CuO.
- 5. Connect the stopper and glass tube (OD = 5 mm, ID = 3 mm, L = 14 cm) to one end of the reduction tube.
- 6. Clamp the reduction tube at the other open end (a clamp without cork or rubber padding is preferable as the tube may get hot).
- 7. Put down the sash of the fume hood.
- 8. Connect the stopper and glass tube to the hydrogen cylinder with rubber tubing, turn on the gas and adjust to as low a flow as possible from the regulator. Place the stopper at the open end of the reduction tube.
- 9. Check that the hydrogen is coming out of the reduction tube via the longer glass tube by collecting the gas in a micro test-tube and seeing if it burns quietly rather than 'pops' when placed in a Bunsen flame.

- 10. Leave for a further 30 seconds to flush out the air, and light the gas emerging from the hole. Do NOT light the gas before testing it this can cause the whole apparatus to explode.
- 11. Light the Bunsen burner and with the tip of a roaring flame heat the oxide at one end of the pile. After a few seconds the powder will glow and start to turn pink. Chase this glow along the tube for about 30 seconds until the whole of the black oxide has turned to pink copper. Continue to heat the tube for at least another minute to ensure that all the oxide has reacted. Take care that the Bunsen flame does not extinguish the hydrogen flame and be prepared to re-light this flame if it goes out.
- 12. Remove the Bunsen burner and allow the reduction tube to cool with the hydrogen still passing over the copper and the excess gas still burning. This prevents air coming into contact with the hot copper and converting it back to oxide.
- 13. When the tube is cool enough to handle, turn off the hydrogen at the cylinder. Wait until the flame has gone out, and remove the stoppers (Otherwise, as air is drawn into the reduction tube, there will be a loud pop which can be disconcerting).
- 14. Weigh the tube and contents again.

2.3.2 Sample Charging

As previously mentioned, powders have not been studied in depth in irradiation experiments. This is due to a number of complications that arise when irradiating powders, one of which is sample charging. In a solid sample, the entire sample is connected. This allows charge from an incident ion beam to move freely throughout the entire sample, and ultimately into ground. In a powder, the sample consists of many individual grains that are not connected. Especially in a sample with spherical grains, there are few points of contact between the individual grains. This makes it more difficult for charge to move through the sample and reach ground. Therefore, even though copper is conductive, the powder form makes the sample much less conductive, so the grounding that exists in the target chamber to achieve a consistently neutral sample is no longer effective (Ref. [9]). Positive charge from the 20 keV ion beam continuously focused on one part of the sample results in an accumulation of positive charge on the portion of the sample that is hit by the beam. We are defining this area of accumulated positive charge on the sample as the beam spot.

Sample charging is a problem in ion irradiation experiments because a positively charged sample can deflect a positive ion beam. If the beam is deflected, it will not hit the sample and will not sputter any ions, and we will get no data from the experiment.

2.3.3 Electron Flood Guns

Thankfully, sample charging is a problem that effects many other applications in physics, and there exists a tool to combat this problem called an electron flood gun. The flood gun uses a conical beam of electrons directed onto the target simultaneously with the positive ion beam. Ideally, the negative electrons will neutralize the build up of positive charge from the ion beam.

Fig. 7 shows the marks left by both the ion beam and the electron beam on the sample cup. The projection of the electron beam onto the sample is much wider than the ion beam to ensure that the entire area is neutralized.



Figure 7: The sample cup after being irradiated by the ion beam, and hit with electrons from the flood gun. The smaller light mark in the center is due to the ion beam, and the larger darker mark is from the flood gun electrons.

3 SIMION

3.1 Background Information

The beam spot remaining neutral is critical to the experiment, as I explained above. In physics, particles don't always behave as we expect them to, so we want to make sure that the flood gun indeed works as intended. Testing the effectiveness of the ion gun directly in the experiment would be time consuming and difficult to observe, because we don't know what the actual sputtering yield should be. It would additionally require that the apparatus be available to use for testing, and there are many other components of the apparatus that need to be tested, aligned, and calibrated. Therefore, I used an ion trajectory simulation software called SIMION (Ref. [5]) to make basic models of this scenario in order to test the efficiency of the flood gun at a wide range of sample voltages. SIMION uses Maxwell's equations to determine the strength and direction of the electric and magnetic fields at any spatial point in the simulation. I have included the four equations below:

$$\nabla \cdot E = \frac{\rho}{\epsilon_0}$$

$$\nabla \cdot B = 0$$

$$\nabla \times E = -\frac{\delta B}{\delta t}$$

$$\nabla \times E = J - \frac{\delta D}{\delta t}$$

Using these equations, SIMION determines how these fields act upon particles, and derives a trajectory. Maxwell's equations are solely related to the magnetic and electric fields. Though very powerful, this means that the simulation does not account for surface physics. We are unable to determine via this simulation if the electron flood gun will neutralize the sample, we are using it to determine how efficient the flood gun will be at getting electrons to reach the sample at various degrees of sample charging.

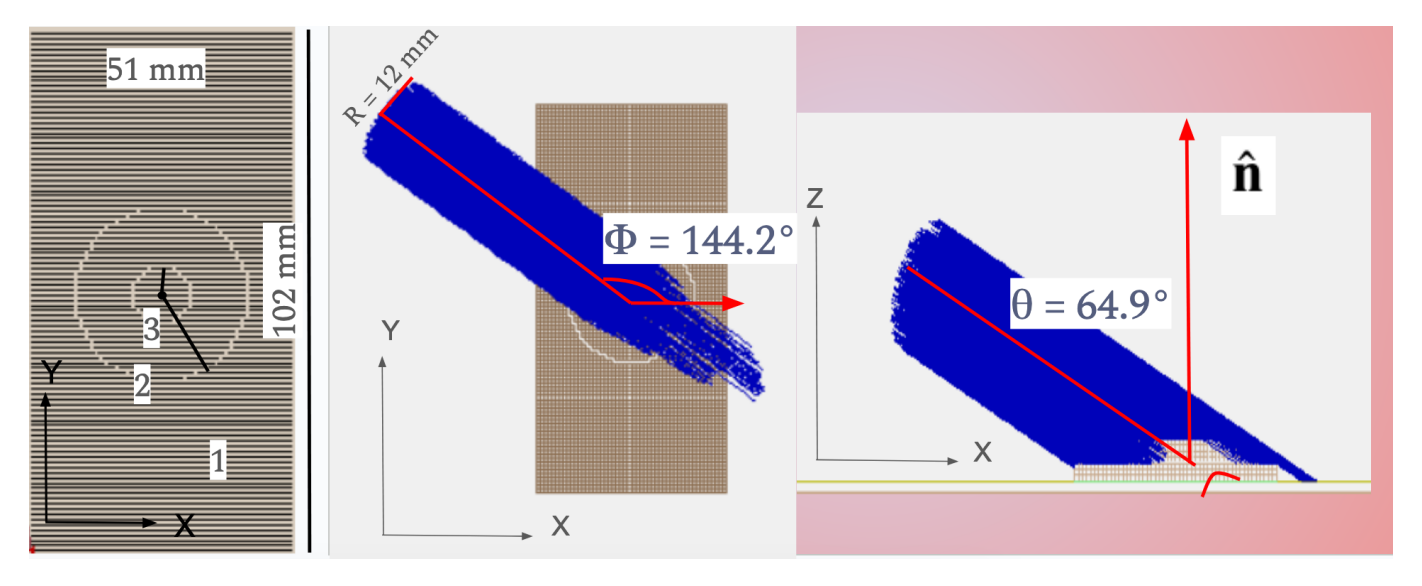


Figure 8: Left: SIMION electrode geometry with dimensions labeled. Middle and Right: trajectories of electron beam onto electrode with 0 volts applied, from the top and side respectively. Provides a visualization of the beam geometry.

3.2 Geometry

When creating a new simulation in SIMION, the first thing to define is the environment, or the 'Potential Array (PA)'. This entails the X, Y, and Z limits, and then the dimensions of any 'electrodes', which are conductive objects in the simulation that have the potential to hold a voltage and generate an electric field.

In my simulation, I created the PA to represent the vacuum space inside the target chamber and the sample holder, which I created out of three different electrodes. The first electrode is the outer rectangle, and it represents the sample stage. The second electrode is the larger circle, and it represents the sample cup and the portion of the sample that the ion beam does not hit: the uncharged portion of the sample. Finally, the third electrode is the center most circle simulates the charged beam spot. All three electrodes have the same dimensions in the simulation as the physical parts that they represent have in the apparatus (Ref. 8). When saving my PA, I utilized the 'fast adjust' format. This allows me to quickly change the voltages of any of the electrodes without having to modify the PA.

Next I define an ion beam to represent the electron beam created by the flood gun. The parameters of the electron beam are listed in Tab. 1.

For simplicity, the beam is cylindrical, with a diameter of 24 mm. This size matches the marks left on the sample cup by the flood gun in the physical instrument shown in Fig. 7

3.3 First Round of Data

I set the voltages for both the second and first electrode to 0 V. Then, I collected data from multiple iterations of the simulation, slowly increasing the voltage of the third electrode, or the beam spot, from 0 - 20k V. The increasing of the beam spot voltage in the simulation represents the accumulation of positive charge on the beam spot from the ion beam in the apparatus. I have included the first four rows of data from one iteration to illustrate the data collection in Tab. 2.

To determine the efficiency of the flood gun, I needed to determine the collection yield of each iteration. I used python to calculate the percent of electrons in each iteration that reach the charged

Parameter	Value		
Number of Particles	1000		
Particle Weight	$0.00054857990946~\mathrm{amu}$		
Charge	-1 e		
Starting KE	-5 eV		
Shape	Cylinder		
Radius	$12\mathrm{mm}$		
Origin	(87.22, 120.55, 32.77)		
Normal Vector	(1, -0.72122, -0.46843)		
Velocity Vector	(1, -0.72122, -0.46843)		

Table 1: SIMION parameters for the electrons in my simulation.

Number	Event	X	Y	\mathbf{Z}	KE
1	4	146.242	73.5149	3	19857.8
1	1	88.1231	121.756	32.8488	5
2	16	199	38.7972	75.1385	21.3905
2	1	83.2423	114.309	33.8944	5

Table 2: Sample data from first round of the simulation, with a beam spot of 20 keV. Number refers to the number of the ion and ranges between 1 to 1000. Event refers to the event that triggered the data collection, for which I selected three; 1 = start of simulation, 4 = electron hits electrode, 16 = ejected electron reaches the edge of the simulation. X, Y, and Z refer to the positional coordinates of the electron at that event, and KE refers to its kinetic energy at that time.

beam spot, and plotted these values against the beam spot voltages so I could visualize how the collection efficiency changes with beam spot voltage. (Fig. 9)

We expected the collection efficiency to reach 100% at a fairly low beam spot voltage, and then remain there throughout the entire range of beam spot voltages. The beam spot is positive and the electrons are negative, therefore it makes sense that the more positive the beam spot, the more electrons it attracts. However, we actually observed that the collection efficiency reaches a maximum at a beam spot voltage of around 1000 V, and then begins to decrease.

We found this result very puzzling, and the majority of my work this summer has been trying to understand why this is happening. Fig. 10 displays sample trajectories. In the trajectories, the electrode starts to eject electrons at high voltages, even though it is positively charged. At very high voltages, the beam follows a spiral path, and the majority of the electrons are ejected from the electrode.

3.3.1 Kinetic Energy Analysis

To test that the simulated results are physically accurate, we examined the kinetic energy of particles that were ejected and particles that hit the beam spot, as displayed in Fig. 11. Sure enough, the particles that do reach the beam spot are accelerated towards it, gaining KE almost to the full value of the beam spot charge. The particles that are ejected remain at their relatively low starting KE. The particles are energetically behaving as expected, which means that from an energy standpoint the simulation is sound.

Collection Efficiency vs Beam Spot Voltage

80

40

100

101

102

103

104

Beam Spot Voltage (eV)

Figure 9: Collection Efficiency vs Beam Spot Voltage for the first round of data collection. Beam Spot Voltage uses a log scale due to the wide range of values. The resulting plot is concave down, with a maximum of around 95% collection efficiency at a beam spot voltage pf about 1000 V.

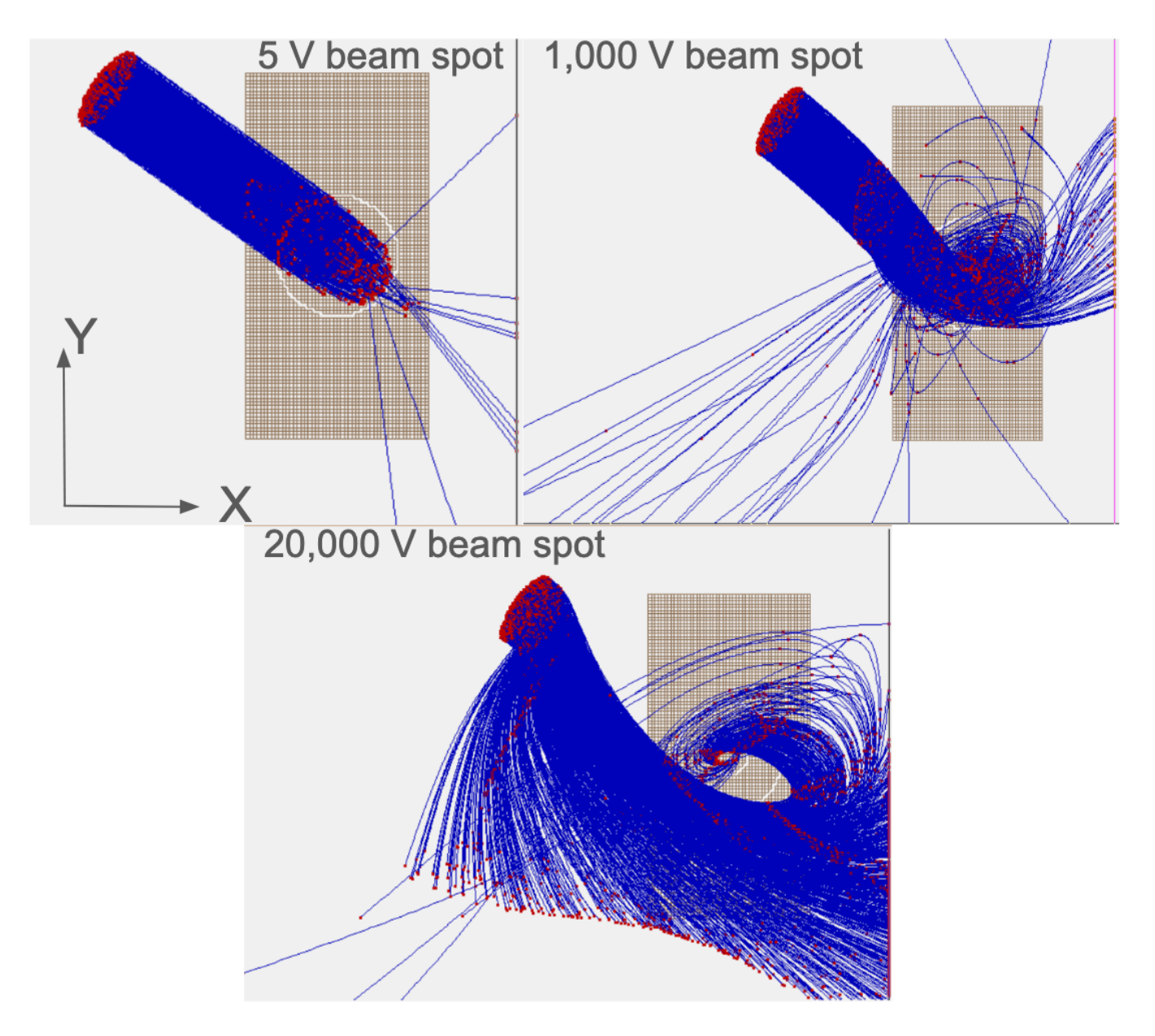


Figure 10: Sample trajectories in the XY plane of the first round of data with beam spot voltages of 5 V, 1000 V, and 20000 V. The electrode is the brown rectangle, and the particle trajectories are indicated by the blue lines. The red squares indicate the start (to the left of each electrode) and finish (various locations) of each electron trajectory.

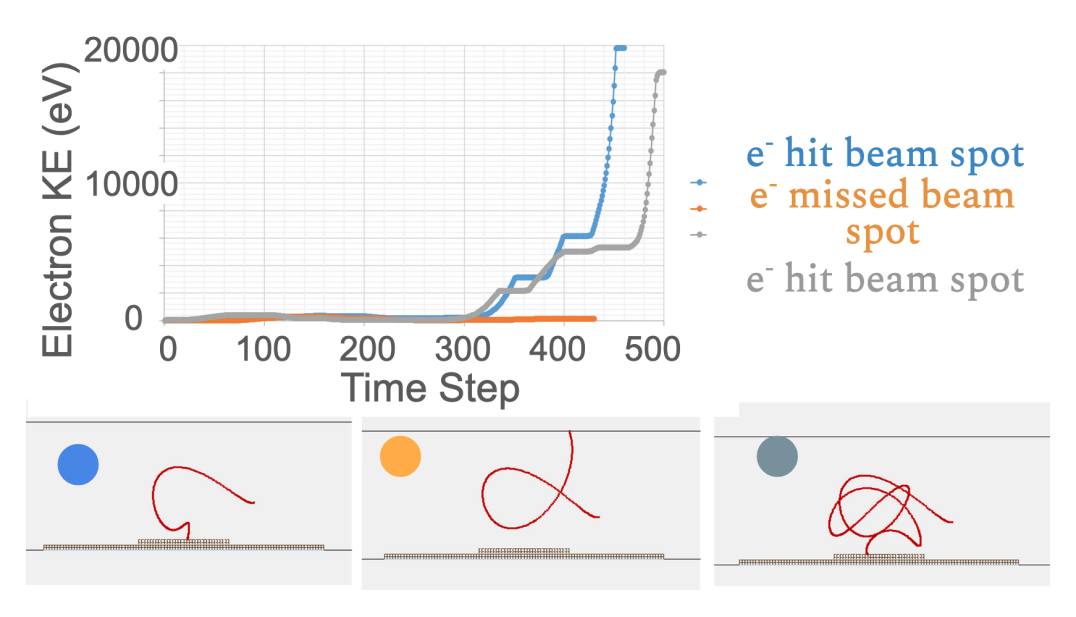


Figure 11: Top: Kinetic Energy vs Time Step of three particles. Bottom: The trajectories of each particle. The two electrons that gain KE were accelerated towards the beam spot by the electric field, and the electron that remains at a low KE was ejected.

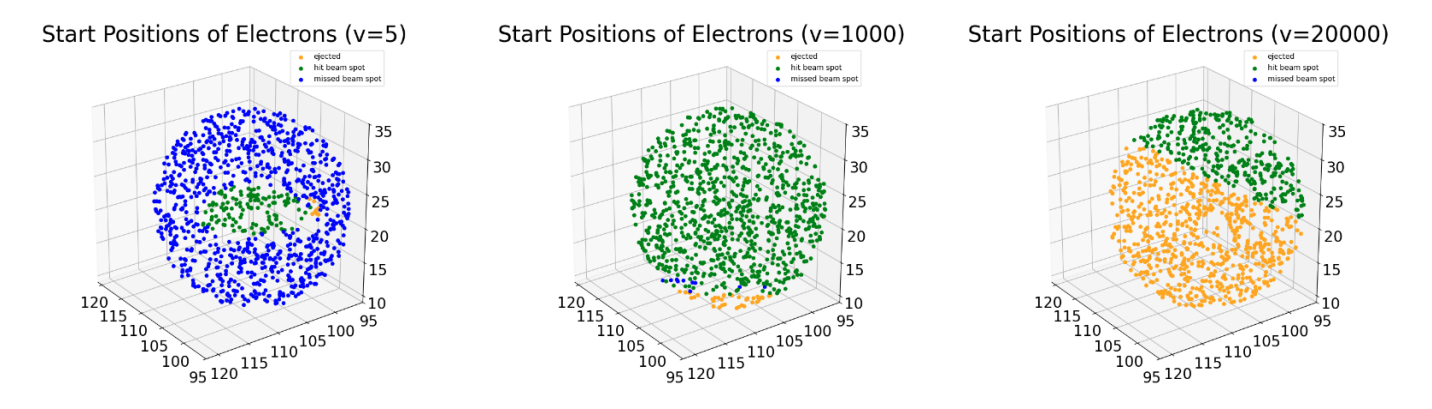


Figure 12: Starting position of electrons in each ion beam, separated by color into ejected (yellow), hit beam spot (green), and missed beam spot (blue).

3.3.2 Positional Correlation

Next we tested if there was some sort of positional correlation. I wanted to visualize where in the original beam the ejected particles were coming from, and if there was some sort of trend we could understand. So I plotted the starting positions of each particle sorted into three groups: hit beam spot, missed beam spot, and ejected. Fig. 12 contains the resulting plots from the three iterations matching the sample trajectories above. The ejected particles come from the edge of the beam at low voltages, and as the voltage increases more and more of the inner beam particles are ejected. At high voltages, more than half the beam is ejected, but only the lower portion of the beam. This identifies a positional relationship between the electrons and the electrode that defines wether or not they are ejected.

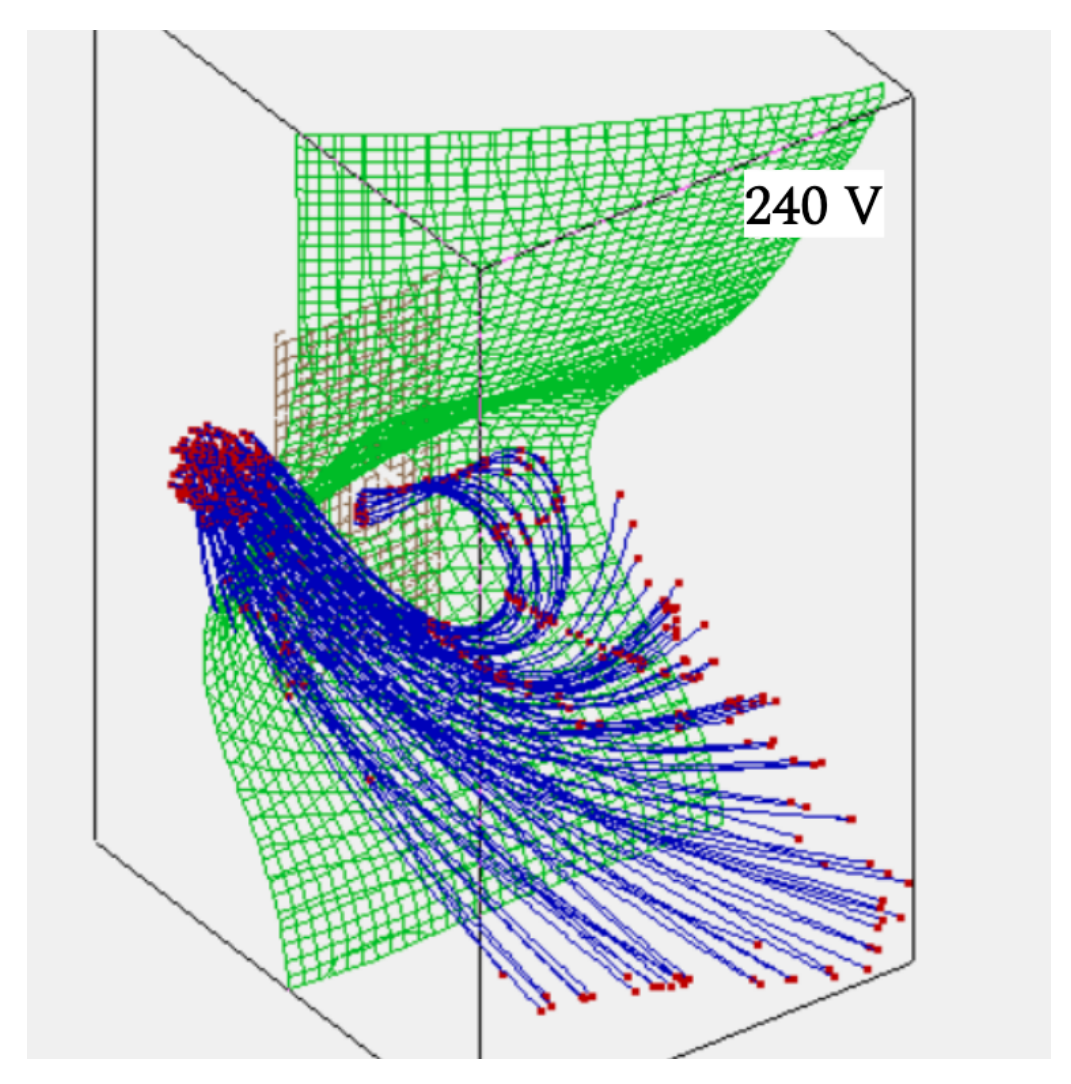


Figure 13: 3d gradient of the electric field at 240 volts in green, with the electron beam in blue.

3.3.3 Electric Field Asymmetry

This positional correlation made me wonder about the symmetry of the electric field. It is symmetrical across the X and Y axis, but it is not symmetrical from the perspective of the beam. Fig. 13 shows 3-D contours of the electric field with the maximum beam spot voltage. The electrons trajectories are bent by the field, the majority of them so bent that they never end up reaching the target. This made me wonder, if we removed asymmetry from the simulation would we still experience these weird results?

This first symmetry test uses a very wide sample plate (Fig. 14). Since the origin of the beam is now within the XY projection of the plate, it no longer experiences any asymmetry relative to the plate. The electric field lines shone in the right image are symmetrical. In this model, with the beam spot at a max voltage of 20 key, all of the electrons reached the sample plate.

The second symmetry test removes asymmetry by aligning the beam perpendicular to the plate, so that the electric field is symmetrical from the beams point of view (Fig. 15). This method of removing asymmetry was also very effective at collecting electrons. With the max beam spot voltage of 20 keV it collected 99% of electrons. Since removing asymmetry from the simulation seems to solve our problem, it is clear that the geometry of the beam has a more significant impact on collection yield than we anticipated. We wondered if there was another location the flood gun could originate

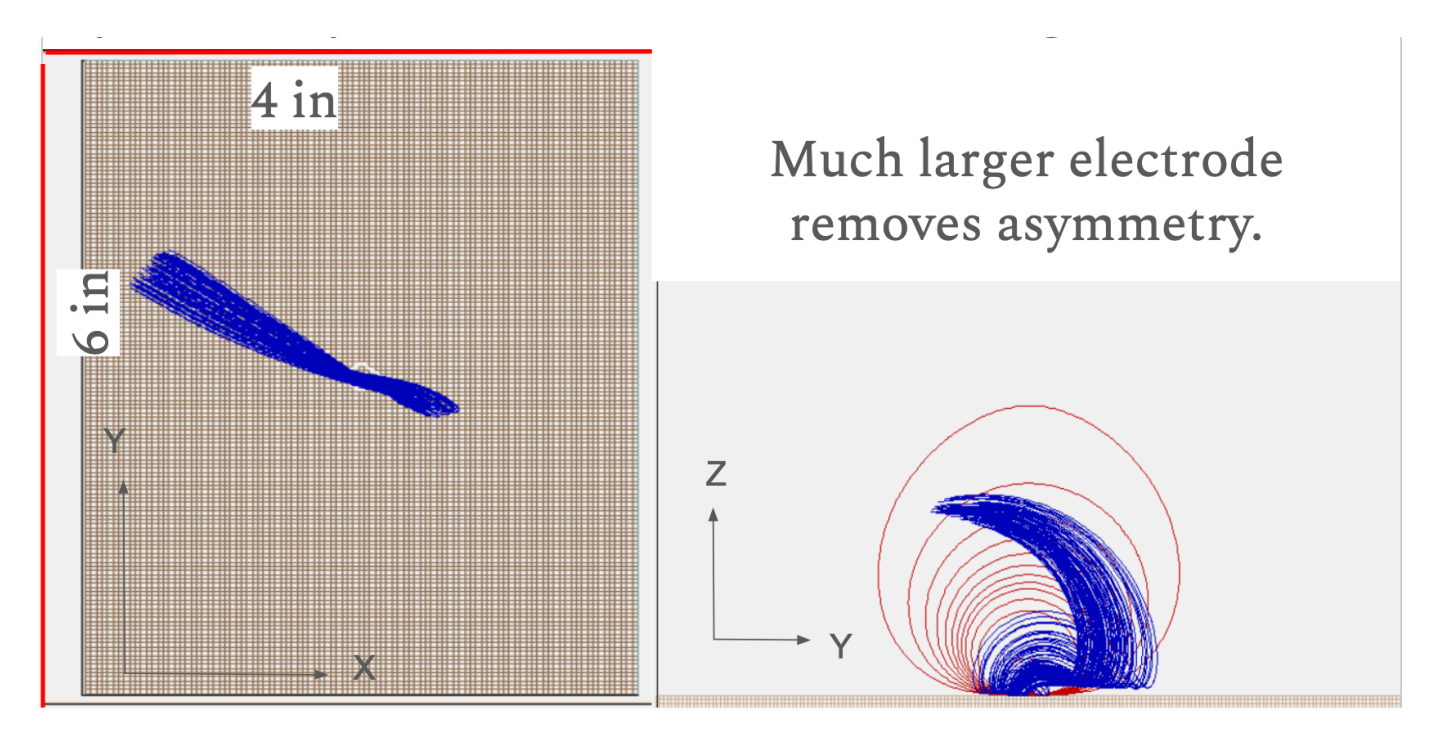


Figure 14: Left: Top view of wide electrode with 20 kV applied to the beam spot and electron beam, with dimensions. The beam partially covers the beam spot from this perspective. Right: Side view of large electrode with 20 kV applied to the beam spot, and the resulting electron beam trajectory. The electric field lines are pictured in red.

from in the experiment that would reduce asymmetry as much as possible.

3.4 Alternate Beam Port

Turns out, there is another port location in the target chamber that is unused by any other equipment. We determined its polar and azimuthal angles, and from this created a new beam in the simulation that originates from this port which is shone projected onto the zero volt electrode in Fig. 16. We repeated the same iteration process we followed with the original beam, and determined that the alternate port does actually have a slightly better collection efficiency, especially at high beam spot voltages (Fig. 17). The electrons that are ejected from this beam are also much closer to the edge of the beam than in the original location, which is depicted in Fig. 18. This leads us to believe that this beam geometry at this location is more ideal.

3.5 Beam Re-Shape

Clearly the beam geometry has more of an impact than we initially anticipated. This made us question the validity of some of the simplifications we made, such as the shape of the beam. We originally modeled it just as a cylinder with a 24 mm diameter for simplicity, since 24 mm is the diameter of the electron beam when it reaches the sample cup. However, the aperture of the flood gun is only about 6.5 mm across, meaning that the electron beam is actually cone shaped. We determined its half angle to be around 10 degrees, and created new beams at both the original and alternate port location that were cone shaped, originating from a 5 mm diameter circle.

We plotted collection efficiency vs voltage for the new beam shapes in Fig. 19, and compared them to these same plots for the old beam shapes. The difference in collection efficiency is quite

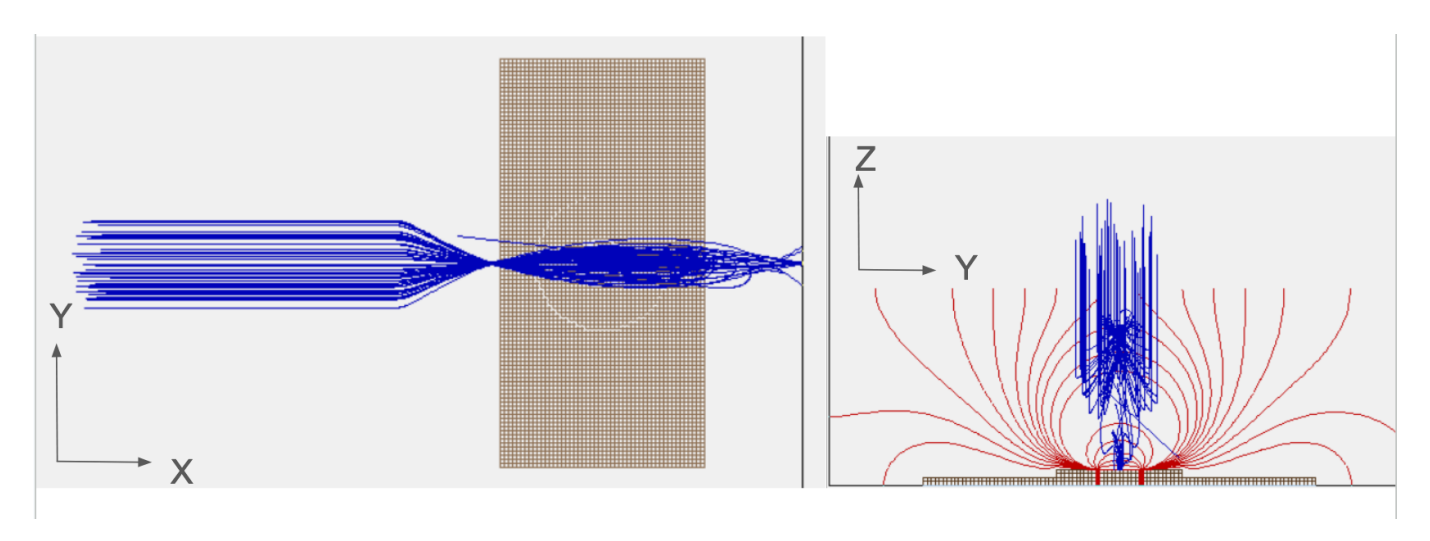


Figure 15: Left: Top view of symmetry test with perpendicular beam. 20 kV is applied to the beam spot. Right: Side view of symmetry test with perpendicular beam. 20 kV is applied to the beam spot. Electric field lines are shown in red.

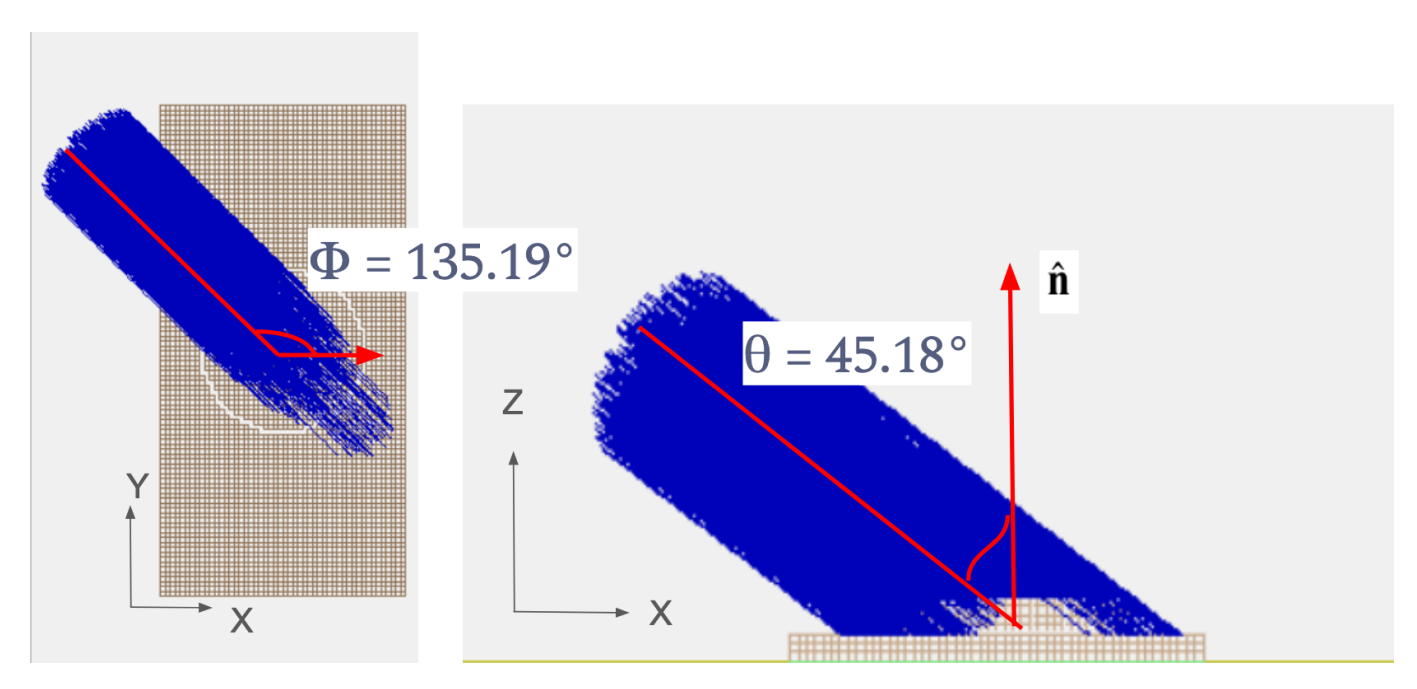


Figure 16: Azimuthal and polar coordinates of the electron beam originating from the alternate electron port. The beam is projected onto a 0 V beam spot, and has a diameter of 24 mm

Collection Efficiency vs Beam Spot Voltage Collection Efficiency (%) 100 80 60 40 20 Original Port Location Alternate Port Location 10¹ 10^{2} 10° 10^{3} 10⁴ Beam Spot Voltage (eV)

Figure 17: Collection Efficiency comparison between the original port (blue) and the alternate port (orange). The alternate port has a slightly better Collection Efficiency, especially at high beam spot voltages.

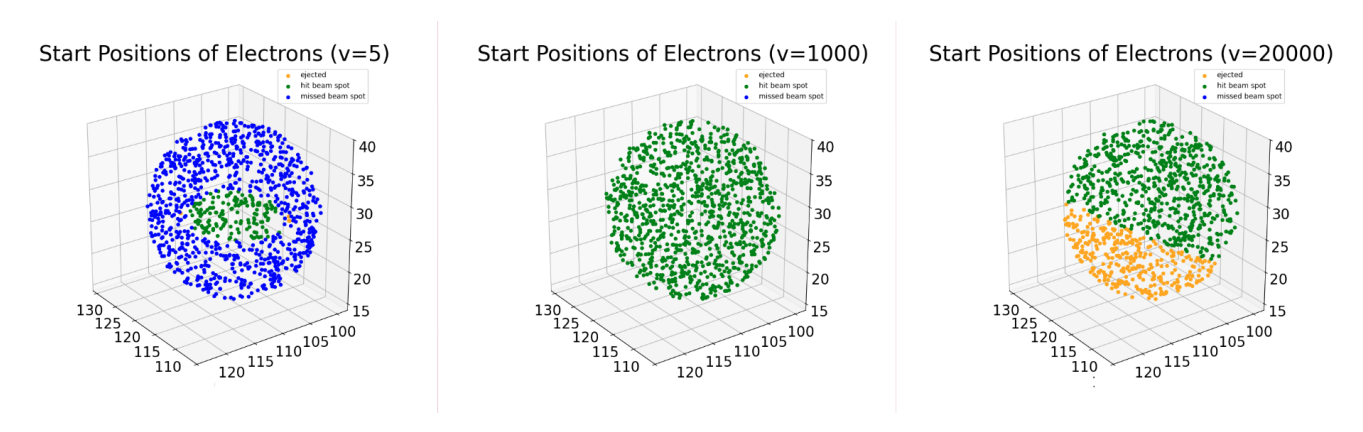


Figure 18: Start positions of the electrons in the alternate beam spot beam, organized by ejected, hit beam spot, and missed beam spot. The start positions of the electrons in the alternate beam follows a similar trend as the start positions of the electrons in the original beam.

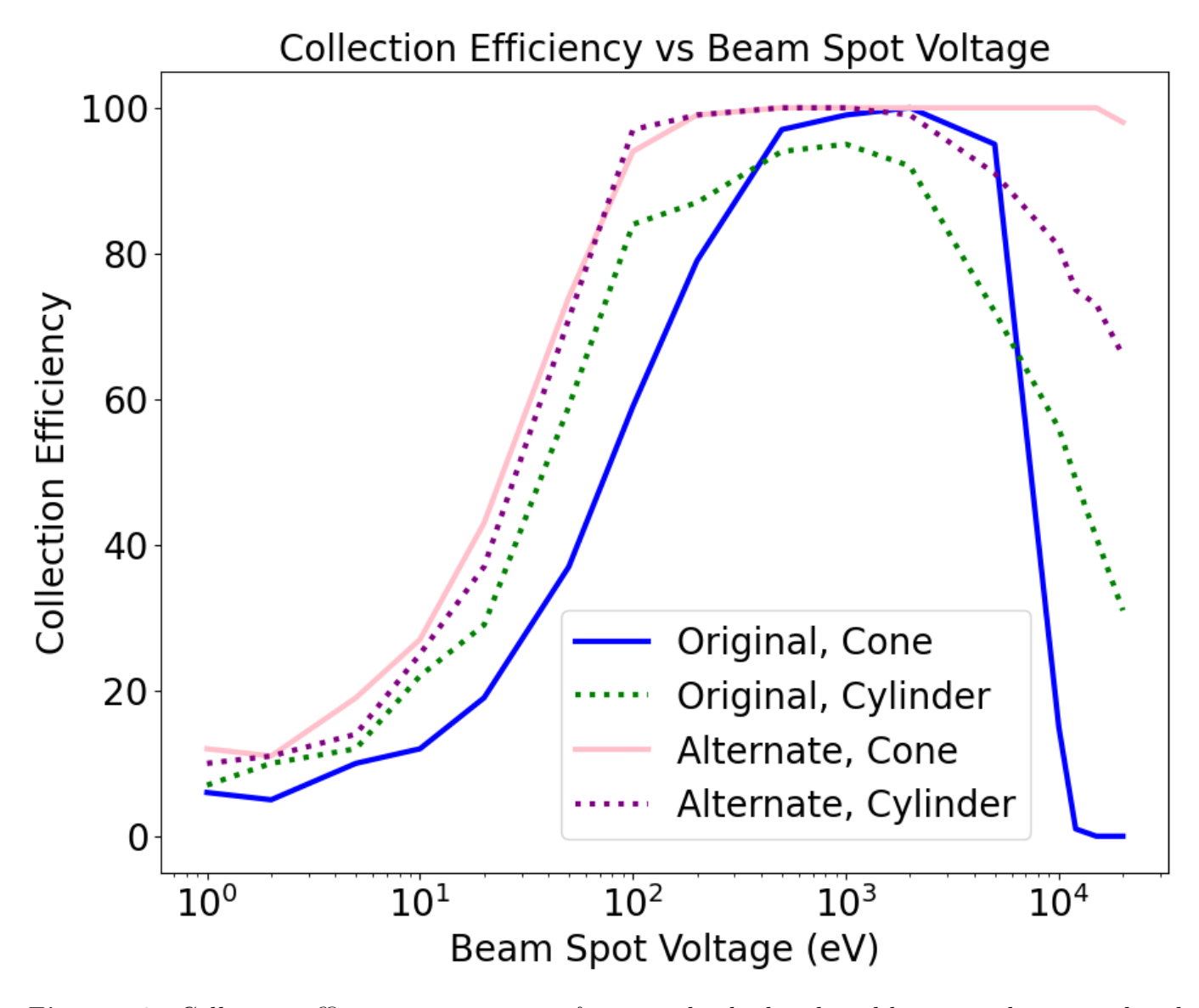


Figure 19: Collection efficiency comparison of cone and cylinder shaped beams at the original and alternate port location. The cone shaped beam originating from the alternate port, shown in pink, has the best collection efficiency, and does not display an extreme decrease at high beam spot voltages.

large, especially with the alternate port location. The collection efficiency does not drop off at the alternate point, but remains at a steady maximum at the highest beam spot voltage. It seems that the over-simplified cylindrical beam was actually amplifying some of the problems we were experiencing due to the asymmetrical electric field. Since the cone beam shape more accurately resembles the flood gun, we believe that these simulation results are closer to reality than the cylindrical beam. Therefore, we determine that the flood gun will be effective at neutralizing the beam spot across the entire range of beam spot voltages at the alternate port, and up to about 15,000 V at the original port.

4 Conclusion

There is a lot of room for improvement in the simulated model. The nature of the 10 week internship meant I had to keep everything relatively simple, so I did not include all of the components in the sample chamber in my model. Components like the dome and the chamber itself are metal and therefore conductive, meaning they would impact the electric field within the sample chamber. If I had more time, a more accurate recreation of the entire target chamber geometry would yield more accurate results from the simulation. Additionally, I only simulated electron beams with a random distribution. The beam profile is a actually more similar to a gaussian distribution, which could also be included in the simulation to improve the results. Although there is room for improvement, my results did have an impact on the overall experiment. It raises the question of moving the flood gun. In theory, the alternate location has a better collection yield. However, as I mentioned before, each part of this instrument has been tediously and precisely calibrated, and moving the flood gun would mean some of these steps have to be repeated, which is time consuming, and opens another source of potential human error. Regardless of where the flood gun originates from, we have determined that the flood gun MUST be turned on before the ion beam enters the target chamber. The electrons are not guaranteed to reach the beam spot when it is highly charged, as we previously anticipated. We need to keep the beam spot charging as low as possible to prevent maximize the amount of electrons that reach the sample.

5 Acknowledgements

This material is based upon work supported by the National Science Foundation under Grant No. PHY-2349438.

References

- [1] C. Bu, B. C. Bostick, K. P. Bowen, S. N. Chillrud, D. L. Domingue, D. E. Ebel, G. E. Harlow, P.-M. Hillenbrand, R. M. Killen, X. Schury, D. Urbain, R. Zhang, and D. W. Savin. Laboratory simulations of solar wind ion irradiation on the surface of mercury. *Lunar and Planetary Science Conference*, 2021.
- [2] D. L. Domingue, C. R. Chapman, R. M. Killen, T. H. Zurbuchen, J. A. Gilbert, M. Sarantos, M. Benna, J. A. Slavin, D. Schriver, P. M. Tr´avn´ıˇcek, T. M. Orlando, A. L. Sprague, D. T. Blewett, J. J. Gillis-Davis, W. C. Feldman, D. J. Lawrence, G. C. Ho, D. S. Ebel, L. R. Nittler, F. Vilas, C. M. Pieters, S. C. Solomon, C. L. Johnson, R. M. Winslow, J. Helbert, P. N. Peplowski, S. Z. Weider, N. Mouawad, N. R. Izenberg, and W. E. McClintock. Mercury's Weather-Beaten Surface: Understanding Mercury in the Context of Lunar and Asteroidal Space Weathering Studies. Space Sci. Rev., 181:121–214, 2014.
- [3] D. Gamborino and P. Vorburger, A. Wurz. Mercury's subsolar sodium exosphere: an ab initio calculation to interpret MASCS/UVVS observations from MESSENGER. *Ann. Geophys.*, 37:455–470, 2019.
- [4] R. M. Killen, M. H. Burger, and R. J. Cassidy T. A. Vervack, Jr. Understanding Mercury's Exosphere: Models Derived from MESSENGERS Observations. *Cambridge University Press*, pages 407–429, 2018.
- [5] D. Manura and D. Dahl. SIMION (R) 8.0 User Manual. Adaptas Solutions.
- [6] T. J. McCoy, P. N. Peplowski, and S. Z. McCubbin, F. M. Weider. The Geochemical and Mineralogical Diversity of Mercury, Mercury: The View after MESSENGER. in Solomon, S. C., Anderson, B. J., Nittler, L. R. (eds.), Cambridge University Press, page 176–190, 2018.
- [7] A. E. Potter, R. M. Killen, and T. H. Morgan. The sodium tail of Mercury. *Meteorit. Planet. Sci.*, 37:1165–1172, 2002.
- [8] A. E. Potter, R. M. Killen, and T. A. Reardon, K. P. Bida. Observation of neutral sodium above Mercury during the transit of November 8, 2006. *Icarus*, 226:172–184, 2013.
- [9] Mizuki Shoyama and Shuji Yoshioka, Hironobu Matsusaka. Particle charging and levitation using UV irradiation and electrostatic field. *IEEE Industry Applications Society*, 2020.
- [10] I. Yoshikawa, O. Korablev, S. Kameda, D. Rees, H. Nozawa, S. Okano, V. Gnedykh, V. Kottsov, K. Yoshioka, G. Murakami, and G. Ezawa, F. Cremonese. The Mercury sodium atmospheric spectral imager for the MMO spacecraft of Bepi-Colombo. *Planet. Space Sci.*, 58:224–237, 2010.